Modeling the Peano fluidic muscle and the effects of its material properties on its static and dynamic behavior

2016 Smart Mater. Struct. 25 065014

(http://iopscience.iop.org/0964-1726/25/6/065014)

IOP Publishing Smart Materials and Structures
Smart Mater. Struct. 25 (2016) 065014 (16pp) doi:10.1088/0964-1726/25/6/065014

Modeling the Peano fluidic muscle and the effects of its material properties on its static and dynamic behavior

Allan Joshua Veale[1,2], Sheng Quan Xie[1] and Iain Alexander Anderson[2]

[1] Department of Mechanical Engineering, The University of Auckland, New Zealand
[2] The Biomimetics Lab, Auckland Bioengineering Institute, The University of Auckland, New Zealand

E-mail: avea007@aucklanduni.ac.nz, s.xie@auckland.ac.nz and i.anderson@auckland.ac.nz

Received 26 November 2015, revised 19 April 2016
Accepted for publication 20 April 2016
Published 13 May 2016

Abstract

The promise of wearable assistive robotics cannot be realized without the development of actuators that mimic the behavior and form of biological muscles. Planar fluidic muscles known as Peano muscles or pouch motors have the potential to provide the high force and compliance of McKibben pneumatic artificial muscles with the low threshold pressure of pleated pneumatic artificial muscles. Yet they do so in a soft and slim form that can be discreetly distributed over the human body. This work is an investigation into the empirical modeling of the Peano muscle, the effect of its material on its performance, and its capabilities and limitations. We discovered that the Peano muscle could provide responsive and discreet actuation of soft and rigid bodies requiring strains between 15% and 30%. Ideally, they are made of non-viscoelastic materials with high tensile and low bending stiffnesses. While Sarosi *et al*'s empirical model accurately captures its static behavior with an root mean square error of 10.2 N, their dynamic model overestimates oscillation frequency and damping. We propose that the Peano muscle be modeled by a parallel ideal contractile unit and viscoelastic element, both in series with another viscoelastic element.

Keywords: fluidic artificial muscles, actuator, fabrication, Peano muscle modeling, McKibben muscle, static and dynamic behavior, material properties

(Some figures may appear in colour only in the online journal)

1. Introduction

There is a fundamental need for actuation systems appropriate for wearable assistive robotics. These robots have the potential to restore motion to people with physical disabilities [1, 2] and work with therapists to increase the affordability and accessibility of rehabilitation for those with mobility impairments . However, there is a gap between actuator technologies designed for assembly line environments and actuators for robots that can function safely, effectively, and robustly on the body of a human in the uncertainty of a real-world environment. Wearable actuators should be slim, powerful, and compliant to ensure the unobtrusive, effective, and safe assistance of their wearer [3]. In contrast, traditional hydraulic, pneumatic, and electric actuators have been matured in highly predictable industrial environments requiring precise and powerful motion but with few constraints on form and portability. Hence, traditional actuators are considered relatively rigid programmable position sources unable to inherently deal with dynamically changing surroundings and soft surfaces. These are abilities that humans take for granted, but limit traditional actuators' suitability for effective wearable assistive robotics.

Researchers working to bridge this gap have naturally drawn inspiration from the characteristics of biological mammalian muscles, which are designed to perform very well in the real world, to create various kinds of artificial muscles. Fluidic muscles or pneumatic artificial muscles (PAMs) are a kind of artificial muscle that generate high forces and have an elastic behavior comparable to biological muscles. Traditional

PAMs such as the McKibben PAM and Pleated PAM (PPAM) have a cylindrical form that inflates outwards and contracts along its length as shown in figures 1(a) and (b). The more popular elastomer bladder McKibben PAMs also have significant threshold pressure and hysteresis compared to Daerden's PPAM [4]. However, they have a minimum surface area and hence force producing potential for their initial, uninflated volume (deadvolume) because of their circular cross-section. This deadvolume does not contribute to the muscle's energy output [5]; slows it down [6]; and requires an increase in muscle diameter or multiple parallel muscles to increase force [7]. Unfortunately, these latter two factors increase the muscle actuator's thickness and complexity respectively. The Peano muscle aims to reduce the deadvolume of these fluidic muscles for space critical applications such as wearable robots, with the additional benefits of a completely soft construction and a low threshold pressure. It consists of a series of flexible airtight tubes connected along their lengths and loaded parallel to their diameter (figure 1(c)). When inflated, each tube contracts from its flat width of w_0 by Δw so that the muscle exerts a force on its load.

Peano muscles are a new type of fluidic muscle and this paper contributes foundational research into their modeling, design, and materials optimization. First proposed by Sanan *et al* [8] in 2013 as the linear Peano actuator, they have also been referred to as the Pouch motor and flat PAM. Work has been presented on their fabrication [9, 10], modeling [10, 11], and application to an orthosis [12] and a robotic manipulator [9]. Here we apply Sarosi's accurate empirical PAM model [13, 14] to the quasistatic and dynamic modeling of the Peano muscle. We introduce several new fabrication techniques and the concept of the slanted weave (SW) Peano muscle. Lastly, we investigate the effect of the Peano muscle's material properties on its static and dynamic performance, as has been done for PAMs [15, 16], and discuss its future application. While Niiyama *et al* [17] and Chang *et al* [18] have characterized the effect of geometry on Peano muscles' static behavior and recognized the dependence of muscle performance on muscle material tensile stiffness, the effect of Peano muscles' material on their behavior is unstudied. This research is important because it firstly highlights the capabilities and limitations of the actuator concerning its potential application in wearable actuation and other soft robotics systems. Secondly, it provides insight for future modeling and optimization into how the actuator's material properties influence its performance characteristics.

In the next section of this paper we present the empirical modeling of the Peano muscle. Section 3 introduces Peano muscle fabrication techniques. Following sections describe an experimental study on Peano muscle materials; discuss the findings of this study on the application, optimization, and modeling of the Peano muscle; and overview the key contributions of the paper.

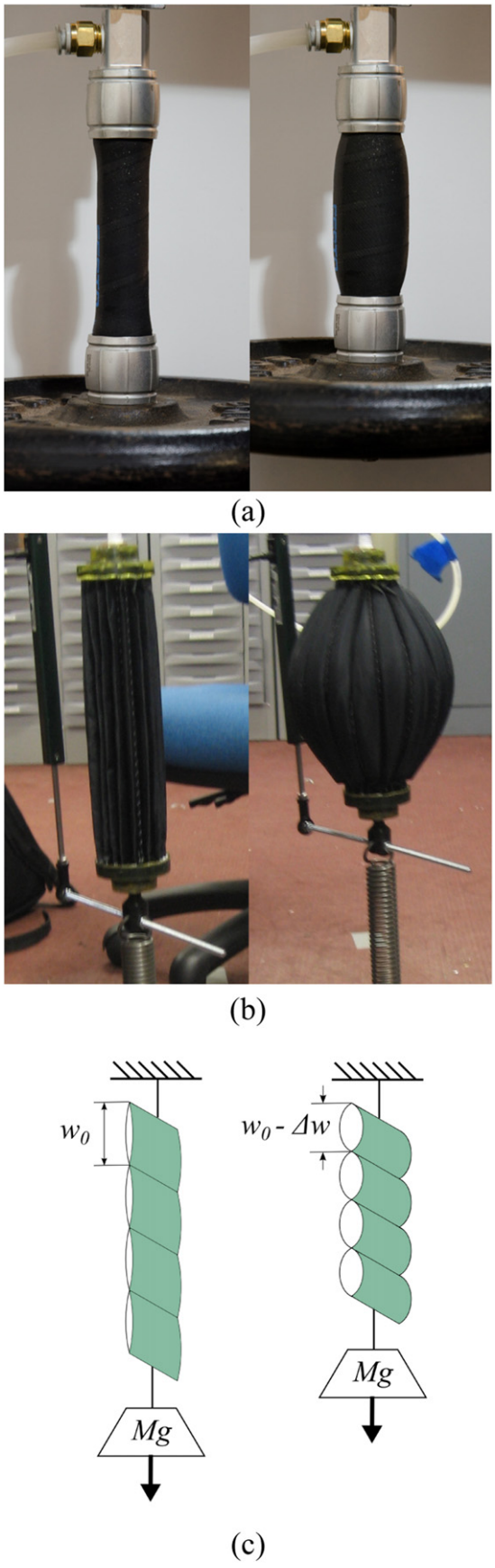

Figure 1. Operating principle of the McKibben PAM (a) PPAM (b) and Peano muscle (c).

2. Muscle modeling

While dynamic models exist for PAMs, only the static behavior of Peano muscles has been modeled. In this section we review these static Peano muscle models and then evaluate the ability of Sarosi *et al*'s [14] dynamic PAM model to capture the static and dynamic behavior of Peano muscles. Currently, virtual work [11] and force balance [10] methods have been proposed to model the static force generation of the Peano muscle. These physics-based models of an ideal Peano muscle with infinitely stiff and infinitely flexible muscle tubes show that it generates an infinite blocking force (the force generated by the muscle when it is fixed at its deflated length and pressurized) and maximum contractile strain (free-strain) of about 36%. Note that the terms stiff and flexible are used in this paper in the sense that such an ideal muscle has an infinite tensile stiffness and zero bending stiffness respectively. Its force is also proportional to its pressure and the planar area of the deflated muscle tubes. Real Peano muscles have finite blocking forces and lower free-strains that reflect the non-negligible tensile and bending stiffnesses of their tube material. To account for the effect of the muscle tubes' tensile stiffness, Niiyama *et al* [11] added a corrective coefficient so that the model could be fitted to force–strain data at a given pressure. Veale *et al* [10] proposed a model based on an approximation of the ideal model that directly incorporated the muscle material's tensile and bending stiffnesses to predict a finite blocking force. However, neither Niiyama *et al*'s or Veale *et al*'s models accounts for the hysteresis effect, muscle material viscoelasticity, or muscle dynamics. Nor can the models be explicitly calculated from the muscle's current pressure and strain.

2.1. Sarosi empirical dynamic model

McKibben PAMs exhibit similar behavior to Peano muscles, hence Sarosi *et al*'s [14] dynamic PAM model is a good starting point for modeling the dynamic behavior of the Peano muscle. Sarosi *et al*'s model is accurate at modeling the static behavior of McKibben PAMs and is empirical, not relying on PAM specific geometry features. This means it can be applied to the Peano muscle. After Reynolds *et al* [19], the model assumes that the muscle can be represented by a force generating contractile element in parallel with a damper. The contractile and damping elements are then in series with an inertial mass m, giving the force balance:

$$\sum F_{\mathrm{y}} = m\ddot{y}, \tag{1}$$

$$F_{\mathrm{ceu}}(p, \varepsilon) - B(p, \varepsilon)\dot{y} - mg = m\ddot{y}, \tag{2}$$

where F_{ceu} is the force generated by the contractile element as a function of the muscle pressure p and contractile strain ε; B is the damping element; and y the muscle contractile displacement related to its strain by the sum of the muscle tubes widths, l_0:

$$y = l_0\varepsilon. \tag{3}$$

Table 1. Coefficients of Sarosi's model fitted to the lower and upper static force data of a Peano muscle.

Coefficient	Lower curve value (i = l)	Upper curve value (i = u)
$a_{i,1}$	16.524×10^{-5}	8.6607×10^{-5}
$a_{i,2}$	20.6623	36.9905
$a_{i,3}$	−51.9497	−42.7436
$a_{i,4}$	-2.9233×10^{-3}	-3.2994×10^{-3}
$a_{i,5}$	4.1291×10^{-4}	4.656×10^{-4}
$a_{i,6}$	−2.109	0.25999

Within this lumped parameter framework, the two part contractile element is defined by Sarosi [13] in equations (4) and (5). These equations are fitted separately to the upper and lower hysteresis curves of force–strain data to predict the upper and lower contraction forces F_{ceu} and F_{cel} respectively.

$$F_{\mathrm{ceu}}(p, \varepsilon) = (a_{\mathrm{u},1}p + a_{\mathrm{u},2})\mathrm{e}^{a_{\mathrm{u},3}\varepsilon} + a_{\mathrm{u},4}p\varepsilon + a_{\mathrm{u},5}p + a_{\mathrm{u},6}, \tag{4}$$

$$F_{\mathrm{cel}}(p, \varepsilon) = (a_{\mathrm{l},1}p + a_{\mathrm{l},2})\mathrm{e}^{a_{\mathrm{l},3}\varepsilon} + a_{\mathrm{l},4}p\varepsilon + a_{\mathrm{l},5}p + a_{\mathrm{l},6}. \tag{5}$$

The damping element is given as:

$$B(p, \varepsilon) = 2\zeta(p)\sqrt{|k(p, \varepsilon)|\, m}, \tag{6}$$

where the muscle tensile stiffness k is based on the gradient of F_{ceu}:

$$k(p, \varepsilon) = (a_{\mathrm{u},3}(a_{\mathrm{u},1}p + a_{\mathrm{u},2})\mathrm{e}^{a_{\mathrm{u},3}\varepsilon} + a_{\mathrm{u},4}p\varepsilon)/l_0 \tag{7}$$

and the pressure dependent Lehr's damping coefficient ζ calculated as:

$$\zeta(p) = \frac{U_{\mathrm{u}} - U_{\mathrm{l}}}{U_{\mathrm{u}}}, \tag{8}$$

where U_{u} and U_{l} are the areas under the upper and lower static force curves between the minimum and maximum strains $\varepsilon_{\min}$ and $\varepsilon_{\max}$ of the muscle at a given pressure p:

$$U_{\mathrm{l}} = \int_{\varepsilon_{\min}}^{\varepsilon_{\max}} F_{\mathrm{cel}}(p, \varepsilon)\mathrm{d}\varepsilon, \tag{9}$$

$$U_{\mathrm{u}} = \int_{\varepsilon_{\min}}^{\varepsilon_{\max}} F_{\mathrm{ceu}}(p, \varepsilon)\mathrm{d}\varepsilon. \tag{10}$$

The minimum strain is zero, or if the muscle can be stretched, slightly less than zero. The maximum strain is the predicted free-strain and calculated by solving $F_{\mathrm{cel}}(p, \varepsilon) = 0$ for ε at the specified pressure.

2.2. Sarosi static model validation and comparison with Veale et al's static model

Sarosi's static force model fits the quasistatic force data from a four-tube Peano muscle best when the muscle is pressurized and improves on the accuracy of Veale *et al*'s non-hysteretic static model. The muscle was loaded at pressures of 0–500 kPa and Sarosi's model fitted with the Levenberg–Marquardt algorithm to give the coefficients in table 1. The model fitted the data with a coefficient of determination of

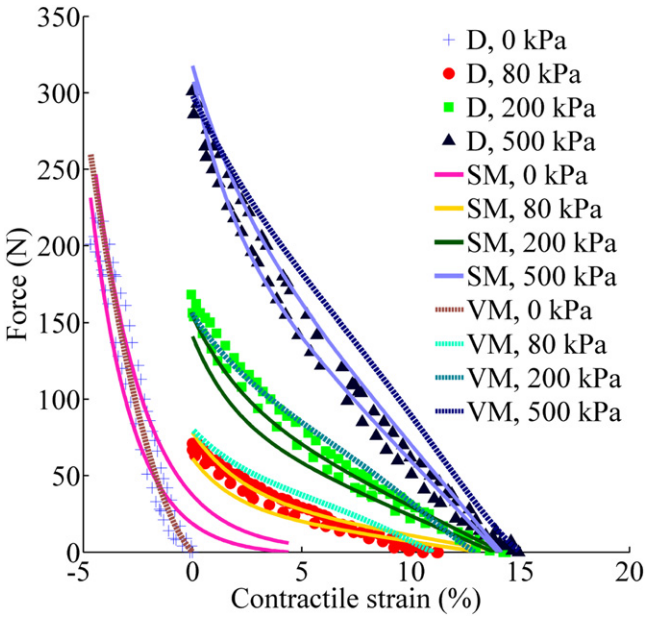

Figure 2. Data (D) and modeled forces with Sarosi's (SM) and Veale's (VM) models for quasistatic tensile loading of a Peano muscle at various pressures.

0.9807, root mean square error (RMSE) of 10.2 N, and maximum error of 37.3 N. In comparison, Veale *et al*'s [10] physics-based model had a higher RMSE of 18.0 N and a higher maximum error of 59.2 N. Figure 2 shows it models the 0 kPa loading cycle data relatively well, but with decreasing accuracy at higher pressures. Its accuracy is further reduced by its inability to capture muscle hysteresis. Veale *et al*'s model is described in [10] and was evaluated here using a muscle with the model geometry and material parameters in table 2. Figure 2 also reveals that the large maximum error in Sarosi's model occurred because, unlike Veale *et al*'s model, the model form does not match the shape of the 0 kPa loading cycle. Repeating the fitting process with data from tests at pressures greater than zero increased the model's accuracy and confirmed that the model works well for static modeling of the Peano muscle for nonzero pressures.

2.3. Sarosi dynamic model validation

Sarosi *et al*'s dynamic model approximately matches the step response of a Peano muscle, but overestimates oscillation frequency and damping. The Peano muscle from the previous section was loaded with an inertial mass of 42 N and its contractile strain recorded in response to pressure steps from 80 to 500 kPa. MATLAB's (R2012b, MathWorks, MA) 'ode45' function was used to solve equation (2) and obtain the response in figure 3. Over the period of a 5% settling time the model had a coefficient of determination of 0.6435, RMSE of 2.6% strain, and maximum error of 15% strain. While the model captured the steady-state strain well, it had a higher oscillation frequency and did not accurately represent the nonlinear nature of the muscle's damping. Sarosi *et al*'s model would be appropriate as a first approximation of the Peano muscle dynamics. However, nonlinear and possibly bidirectional damping terms such as those used in the modeling of McKibben PAMs by Cao *et al* [20] and Tondu [21] would be required to increase its accuracy.

Table 2. Geometry and material parameters of Veale's model, using definitions described in [10].

Parameter	Parameter value
w	0.015 m
l	0.046 m
h	0.002 m
b	0.002 725 m
$A1$	4.085×10^{-4} m^2
$A2$	0.92×10^{-4} m^2
$k1$	$5 \times 10^4 + \sqrt{2.5 \times 10^9 + 388.9 \times 10^6 F}$
$k2$	$1.625 \times 10^{15} t^4 + 1.674 \times 10^6 \times \lvert t \rvert$

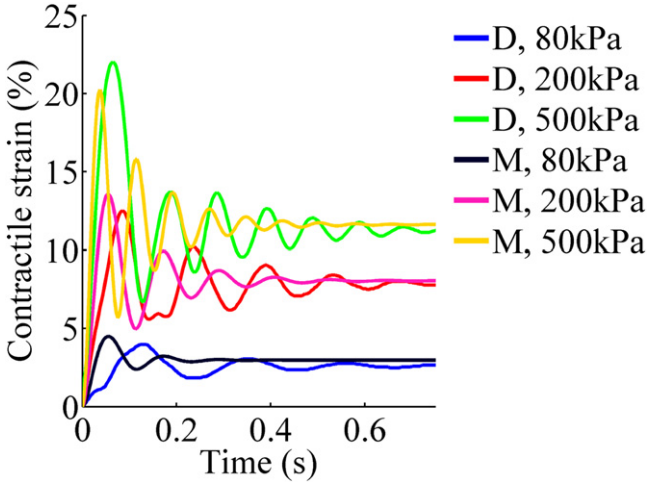

Figure 3. Data (D) and modeled (M) contractile strain for the step response of a Peano muscle loaded with 42 N.

3. Muscle fabrication

Peano muscles are simpler to automatically fabricate than McKibben PAMs in a lab environment [9]. Unlike the tubular form of PAMs, the planar package of the Peano muscle lends readily to layer based fabrication using common rapid prototyping tools such as computer-numerical-control gantries and three-dimensional (3D) printers. The fiber-reinforced tubes of PAMs are commonly made of latex or silicone [16, 22], and polyester or Kevlar for the fibers [23]. Often these components are separate, but they have also been formed as a composite. Peano muscles have been fabricated from thermoplastics as well as elastomers and fibers with welding and casting techniques. Sanan *et al* [8] developed a rotary Peano muscle from a textile reinforced flexible hose woven through sewn fabric tubes. Niiyama *et al* [9, 11, 17, 24] have reported Peano muscles made from two layers of heat bonded thermoplastic sheets with the aim of a customizable and simple fabrication process. So far, they have tried PVC, nylon, polyethylene, and aluminized PET

thermoplastic laminates with thicknesses of 0.028–0.102 mm. The sheets have been welded manually using a line sealer or custom-made heated stamp, and welded automatically using a soldering iron mounted to a 3D computer controlled gantry. In the latter two welding methods, polytetrafluoroethylene (PTFE) coated glass-fiber cloth was used to prevent the plastic from sticking to the heating element. Park *et al* [12] constructed a composite fiber-reinforced elastomer Peano muscle with a zero deadvolume in the deflated state for a compact physical form. It was fabricated from layers of silicone embedded with longitudinal inelastic Kevlar fibers, again for easy 2D layer fabrication. The fiber reinforcement did not constrain the radial expansion of the muscle tubes, so that unlike Niiyama *et al*'s [9] Peano muscles, it bulged outwards when inflated. For this reason, it can be classified as a hybrid of the Baldwin PAM and Peano muscle concepts. Veale *et al* [10] presented a Peano muscle fabricated from a flat textile-reinforced elastomer tube terminated by metal clamps at either end. Aluminum bands were spaced evenly along the flexible body of the muscle to constrain it so that when inflated, it formed a row of tubes.

Thermoplastic materials lend themselves to Peano muscles with a higher free-strain, but lower robustness than composite muscles. The high flexibility of Niiyama *et al*'s [9] lightweight thermoplastic muscles has the advantage of producing a blocking force of 110 N and free-strain approaching 30% at 40 kPa. Their test muscle had three tubes made of 0.102 mm PVC each with a length of 75 mm and a width of 25 mm. While their thin thermoplastic material lends to easy fabrication methods, it has a low puncture and abrasion resistance, and cannot support large forces without permanently deforming. Park *et al*'s [12] muscle consisted of four 14 mm wide by 8 mm long tubes made of 1.75 mm thick fiber-reinforced silicone. It generated 38 N of blocking force and 26% free-strain at 104 kPa. These muscles are more durable, but still relatively vulnerable to failure by puncture or bursting. The lower free-strain is likely due to the reduced flexibility of the thicker muscle tube material and its embedded 0.35 mm diameter Kevlar fibers. As these muscles only have low stiffness along the muscle tube length, they tend to inflate into a sphere, particularly at their 1:0.57 aspect ratio. This causes their elastomer to stretch significantly, storing energy and increasing the surface area over which the fluid pressure acts. Whether these effects are advantageous depends on the Peano muscle's application. Veale *et al*'s [10] Peano muscle had four 17.25 mm wide by 46 mm long tubes about 1 mm thick. It produced a blocking force of about 320 N and free-strain of 17% at 500 kPa. The double layer of textile reinforcement in this muscle in combination with metal components increased its puncture resistance and burst pressure to over 600 kPa. However, compared to Niiyama *et al* and Park *et al*'s Peano muscles, this came at the cost of reduced muscle tube material flexibility, the undesirable use of many rigid components, and a relatively bulky and heavy muscle design.

Given the achievements and limitations of these three implementations of the Peano muscle concept, it has yet to be determined if a soft, puncture resistant, high pressure, and high free-strain muscle design is feasible. This paper will explore the performance of muscles made from thermoplastic and composite materials. Results from the investigation will aid optimization of the Peano muscle for artificial muscle applications with different performance requirements.

3.1. Peano muscles under test

The Peano muscles tested in this paper are in two main categories: those fabricated from a thermoplastic (with and without textile reinforcement) and those from a textile-elastomer composite. Figure 4 shows examples of these muscle types, all with geometries as similar as the different fabrication techniques allow. Regardless of the muscle type, they all have a fluid port, where water enters and exits the muscle, and a bleed port. The bleed port is sealed during muscle operation and is used to bleed all the air out of the muscle and prior to each new testing session. The fluid and bleed ports are secured to hose-like fluid channels either end of the muscles with two copper wire crimps.

The plastic muscles are fabricated from sheets of 60 and 125 μm low density polyethylene (LDPE) welded with a heat impulse sealer in the manner of figure 5. Reinforced plastic muscles are fabricated from the 125 μm plastic preroughened with 600 grit sandpaper. After welding, a 175 g m^{-2} layer of polyester textile is wrapped once around the muscle. A spray adhesive (ADOS Multipurpose Adhesive, CRC Industries NZ, Auckland, New Zealand) bonds the reinforcement to the plastic muscle. The textile's fibers are aligned with the length of the muscle.

The plastic and composite muscles share the same key geometry characteristics shown in figure 5. Namely, the muscle tube width w_t, the muscle tube length l_t, and the channel width w_c. The channel width refers to the size of the fluid passage running along the muscle length. Its normalized form is the percentage ratio of the muscle tube length w_c/l_t.

The composite muscles are made from a silicone elastomer (PlatSil Gel-10, Polytek Development Corp., Easton, PA) reinforced by a polyester or fiberglass textile. Apart from their rigid fluid fittings, they are completely soft and flexible. As seen in a plan view of the muscle (figure 6(a)), they share essentially the same geometry as the plastic muscles. However, their fabrication process requires significantly more effort. Rather than heat welding, the muscles are stitched together with 0.234 mm diameter ultra high molecular weight polyethylene braided cord (14 kg PE Max Power Braid, Tri-Poseidon, China).

Briefly the fabrication can be understood with reference to figure 6(a) and the 3D muscle tube cross-section in figure 6(b). First, a 3 mm thick foam core with the cross-hatched cross-section of the fluid channel is wrapped in a 0.5 mm silicone liner. Spaces between adjacent muscle tubes that receive stitching are filled with silicone. The textile is impregnated with silicone and wrapped once around the muscle so that its fibers are either aligned with the muscle length (a 90-0 weave) or are at 45° to the muscle length (a 45-45 weave). The former weave results in an inextensible muscle and the latter, an extensible (stretchy) muscle called

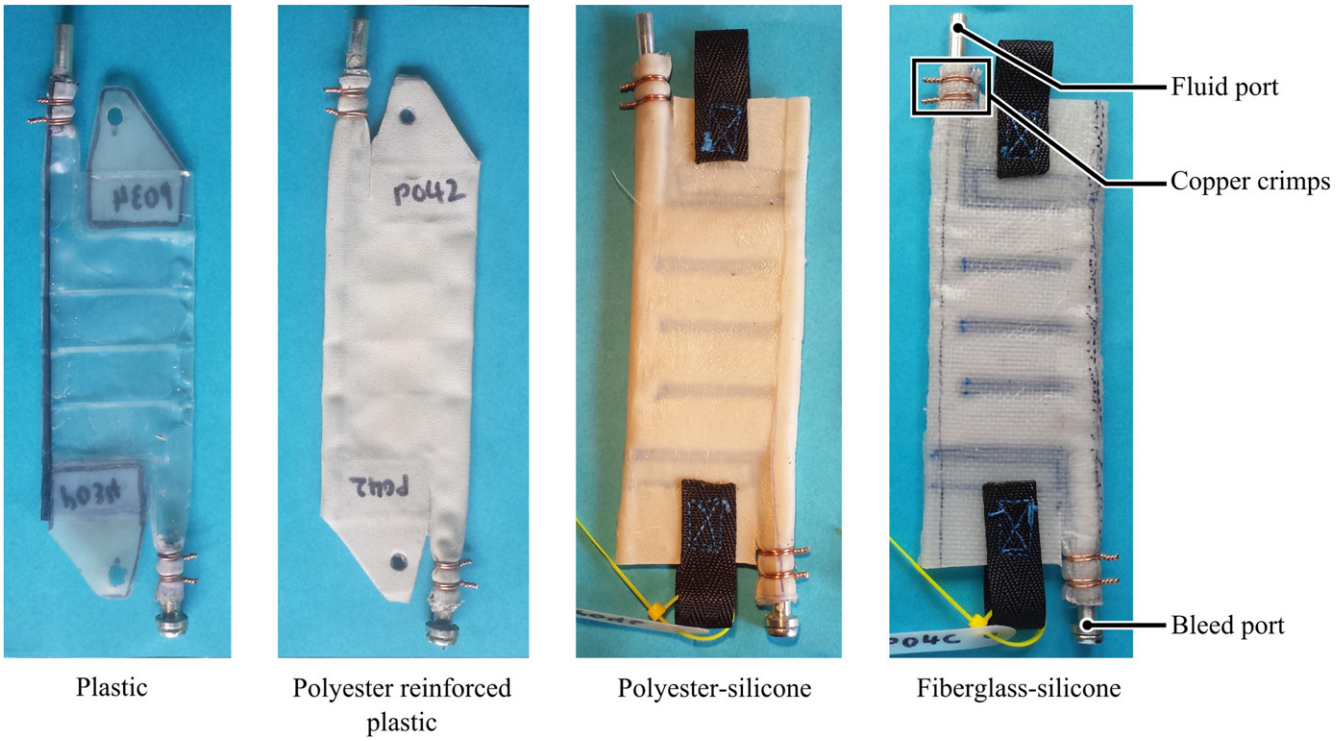

Figure 4. Different types of Peano muscles tested were made from plastic, reinforced plastic, and textile-silicone composites.

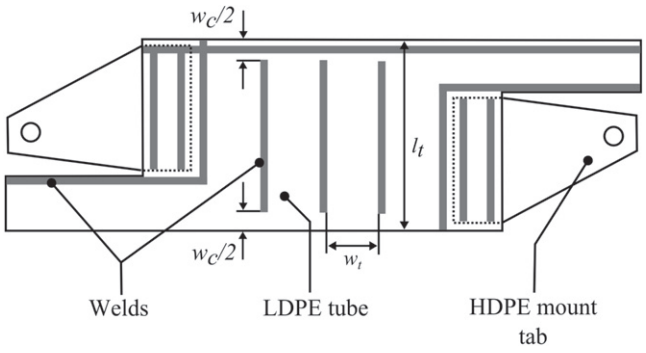

Figure 5. The weld pattern and materials of a plastic Peano muscle. Critical dimensions of the Peano muscle are the muscle tube length l_t, tube width w_t, and channel width w_c.

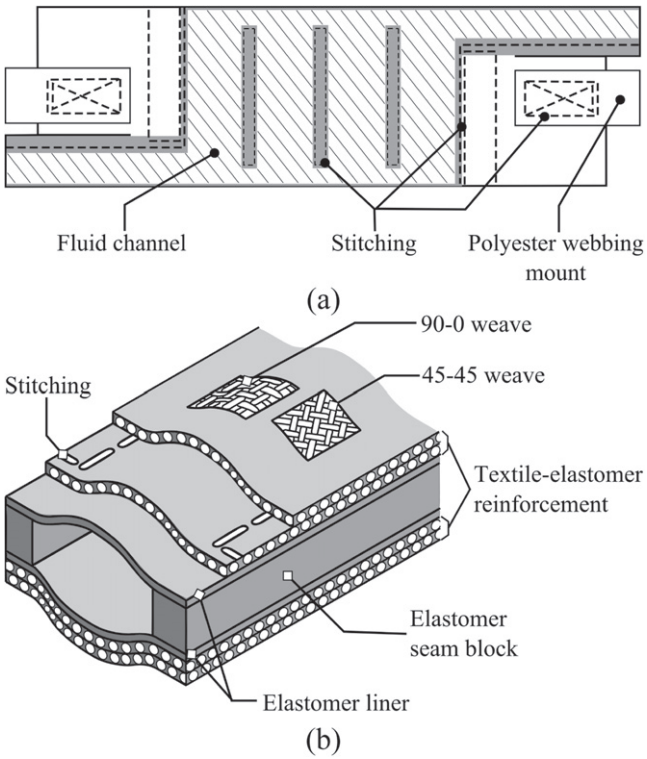

Figure 6. Plan (a) and isometric (b) views of a textile-elastomer composite Peano muscle construction. Although both 90-0 and 45-45 weave cross-sections are shown on a single muscle tube, a real muscle would only feature one weave type.

the SW Peano muscle (see below). Next, the textile is stitched according to the pattern in figure 6(a) and the silicone impregnated textile wrapped around the muscle a second time. Lastly, the foam core is dissolved with a solvent (petrol) and polyester webbing straps are stitched to the ends of the muscles. The small deadvolume introduced by the 3 mm internal height of the uninflated muscle tubes and channels theoretically decreases the force and reduces the flow restriction of these muscles. However, the greater strength of the materials this fabrication technique allows is assumed to outweigh performance differences attributable to the extra deadvolume. Experiments would have to be performed on a new, zero deadvolume composite muscle to ascertain the validity of this assumption. These experiments are outside the scope of this work. Here Peano muscles with two densities of

each textile are tested: 105 g m^{-2} and 175 g m^{-2} polyester and 25 g m^{-2} and 100 g m^{-2} fiberglass.

Clearly, the different combinations of materials and fabrication processes result in wide variation in muscle strength. Consequently, the maximum pressures and loads applied to the muscles were not the same. Test conditions were chosen so that the muscle under test could perform consistently without failing and will be described in section 4.

3.2. SW Peano muscle

Orienting the weave of a textile-elastomer Peano muscle at an angle to the muscle length enables the Peano muscle to be used as a series elastic actuator with a built-in compliance element, like a muscle-tendon unit. We call this type of Peano muscle the slanted weave or SW Peano muscle because of its angled textile fibers. As a hybrid between the Peano and McKibben muscles, we expect it to have the puncture resistance and burst pressure of a standard Peano muscle, but be able to move further and have a reduced tensile stiffness [17]. Its greater range of motion in extension can be exploited by placing SW Peano muscles in antagonistic pairs. This biomimetic actuator configuration has the additional advantage of variable stiffness. When stretched out, the relative displacement of the reoriented textile fibers within the muscle's elastomer matrix may also store significant amounts of elastic potential energy that could be used in dynamic actuation applications. Comparing its behavior to that of an inextensible Peano muscle will form an important part of this study.

4. Effect of material on static and dynamic metrics

Table 3 defines the metrics used to characterize and compare the static and dynamic behavior of the Peano muscles. These metrics were calculated from dynamic step response and quasistatic pressurization and tensile load cycling experiments carried out on the test rig shown in figure 7. This test rig is novel in its ability to hydraulically or pneumatically test both the static and dynamic performance of linear fluidic muscles. In load cycle experiments, an electrohydraulic actuator slowly relaxes and stretches a pressurized muscle. If the actuator is decoupled, fluid flow can be routed through a set of flow restrictors so that the muscle can be gradually pressurized, either locked in position with a brake to measure blocking force, or contracting against an inertial mass M, to measure stroke. Supplying unrestricted fluid flow to the muscle under test allows its dynamic behavior to be characterized through a step response experiment. In a few dynamic experiments, fluid flow through the Venturi tube was not stable enough to measure flow rate and calculate efficiency. However, as metrics were calculated from multiple experiments, efficiency data was always available for a given set of experimental conditions.

The aim of this study was to test how the Peano muscle's material thickness and type affects its static and dynamic behavior. Specifically four-tube, 1:3.3 aspect ratio, and 30% channel width, with the eight materials listed in table 4 were tested hydraulically. After the standard convention, fabrics are specified by their area density, not their thickness. However, in general, a higher area density fabric will be thicker and less flexible for a given fabric material. The muscles were fabricated according to the two techniques outlined in section 3.1 and tested with the experimental conditions described in table 4. Note that the PCS muscle corresponds to the SW Peano muscle concept described in section 3.2. Some of the muscles have different test pressures, inertial masses, and initial tensions for load cycle experiments because of the strength of their materials and the amount of force they can generate.

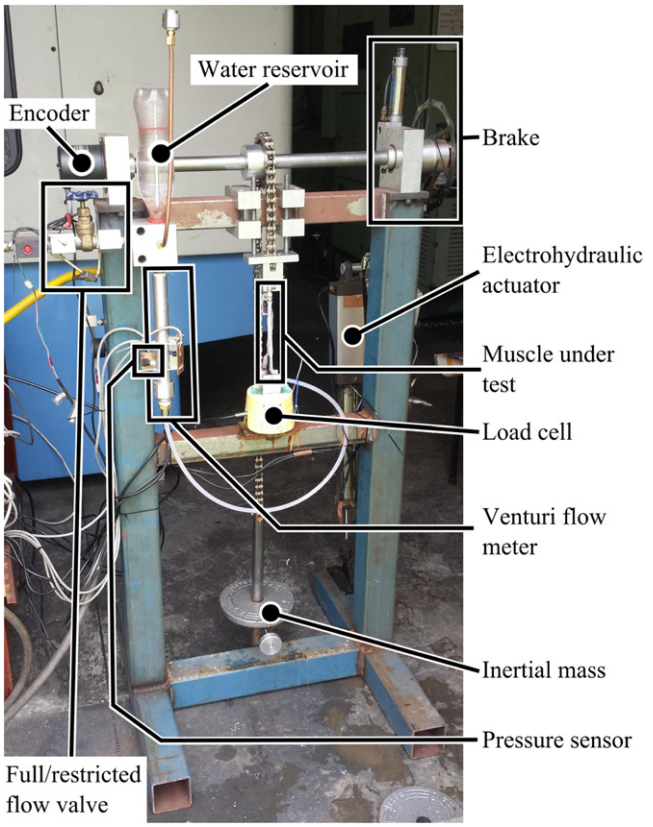

Figure 7. A novel test rig for characterizing the behavior of linear fluidic muscles.

Three repeats of each experiment were carried out on two identical muscles made from each material to capture the effects of natural experimental and fabrication variation. This variation is represented as a shaded area of ±1 standard deviation in line plots or 95% confidence interval bars (Student's t distribution) in bar plots. All plots have the number of repeats designated by n (usually six).

4.1. Results and discussion

The static behavior of the Peano muscles made from plastics and textile-elastomer composites can best be summarized by the load cycle tests in figures 8(a)–(d) respectively. In the unpressurized (0 kPa) load cycle tests of plastic muscles (figure 8(a)), the thicker plastic muscle is stiffer than the

Table 3. Metrics for comparing the Peano muscles' static and dynamic behavior.

Metric	Definition
Blocking force	Force produced by the Peano muscle when pressurized at its unstretched length
Stroke	Distance the Peano muscle lifts a 5.5 N load normalized by its force producing length
Energy	Mechanical work output of the Peano muscle as it contracts quasistatically to its free-strain length
Hysteresis loss	Area between the upper and lower force–strain curves of a quasistatic tensile loading and unloading experiment as a proportion of the area under the upper curve
Speed	Peano muscle root mean square (rms) speed during the time to maximum overshoot of a step response experiment
Power	Rms mechanical power output over the same period that speed is measured in a step response experiment
Efficiency	Ratio of rms mechanical power output to fluid power input over the period that speed is measured in a step response experiment

thinner. Reinforcing the thicker muscle further increases its stiffness. At a strain of −1.5% the stiffnesses of the TP, P, and PR muscles are 1, 2, and 5 kN m^{-1}. At greater negative strains, the stiffness of the unreinforced Peano muscles increases as polymer chains in the plastic straighten, increasing the material stiffness. The pressurized force–strain curves (figures 8(b) and (d)) show that increasing muscle stiffness increases blocking force. They also show that more flexible (and often thinner) muscles have a higher free-strain. While the unreinforced muscles have a similar hysteresis of about 20%–25% (figure 9(a)), the PR muscle has a hysteresis of 50%. The large hysteresis and low free-strain of this muscle can be explained by the stiff viscoelastic nature of the reinforced polyester in bending. The polyester on its own does not have this behavior, but attains it when it is coated with the tacky adhesive that bonds it to the plastic muscle.

Composite Peano muscles (figures 8(c) and (d)) affirm the correlation between increasing material stiffness (as shown in the 0 kPa curves) and increasing blocking force (as shown in figure 8(d)). Fiberglass is stiffer than polyester and higher density versions of the same material are also expected to be stiffer. In contrast, the results here show that the thin fiberglass is less stiff than the non-stretchy polyesters and the lower density polyester stiffer than the higher density polyester. The 0 kPa curves reveal that stiffness increases with muscle extension as fibers in the reinforcement materials align, deforming their elastomer matrices. Pressurized load cycle tests also verify that more flexible muscles (TPC and FC) have a higher free-strain than thicker, less flexible muscles (PC and PCS). Compared to the plastic muscles, the thin fiberglass muscle has a similar stiffness, but less free-strain at a pressure of 30 kPa. Referring also to figure 9(a), the thicker polyester has a higher hysteresis than the thinner, while the two fiberglass reinforcement densities have a similar hysteresis. Hysteresis of the TFC muscle is likely higher as its low-density reinforcement presents a relatively low shear resistance to stitching. This meant that its silicone stretched more, even to the point of breaking some of the glass fibers, increasing hysteretic losses. It is for a similar reason that the TFC Peano muscle had a lower overall tensile stiffness compared to the polyester muscles. It had a free-strain between that of the unreinforced and reinforced plastic muscles at 30 kPa because it is thicker and less flexible than the former, but it is still more flexible than the PR muscle. The higher stiffness of the thinner polyester muscle is because its fabric has a satin weave, but the PC muscle's polyester has a plain weave. Satin weaves are stiffer because their fibers are straighter than those in a plain weave. Investigating the effect of a 45° weave on the behavior of the polyester muscle, the stretchy weave reduces muscle stiffness as expected. Consequently, it produces a lower blocking force but can be extended further than the PC muscle (for a given load).

Figure 9(b) compares the effect of the muscles' materials on their energy output during the load cycle tests of figure 8, as normalized by their test pressures. Among muscles tested at 30 kPa, the unreinforced TP and P muscles had the greatest energy output of about 5.5 J MPa^{-1} followed by the TFC (3.8 J MPa^{-1}) and PR (2.7 J MPa^{-1}) muscles. The remaining muscles were tested at 200 kPa and with the exception of the stretchy polyester muscle, which had an energy output of 4.8 J MPa^{-1}, had an energy output of around 3.2 J MPa^{-1}. As all the Peano muscles share a similar force–strain curve shape, the muscle with the greatest energy output is the one with the optimum balance between a high blocking force and free-strain. Put in material terms, the stiffest, most flexible materials have the greatest energy output. An exception to this is if the muscle has a moderate stiffness with a large recoverable extensile strain as the PCS does. Composite materials with this property can be made by allowing the fibers to rearrange in the elastomer matrix in response to loading. Thus, they can store energy through deformation of the matrix in an ideally uniform manner as possible (to prevent stress concentrations). Some of the muscles tested at 30 kPa exceed the energy output of even the PCS Peano muscle. This is because they have a higher blocking force per unit pressure, as will be explained next.

The blocking forces of the Peano muscles have been normalized by their test pressures of 30 and 200 kPa (figure 9(c)) because an ideal Peano muscle generates a force proportional to its pressure. Considering the trends in the muscle groups at the two test pressures separately, blocking force increases with muscle stiffness. This result is consistent with the load cycle curves of figure 8. More interesting is that the stiffest muscle (FC) tested at 200 kPa has a normalized blocking force of 350 N MPa^{-1}, less than that of the least stiff muscle (TFC or TP) tested at 30 kPa (570 N MPa^{-1}). The reason is that the prototype composite muscle mounts

Table 4. Materials and experimental conditions of Peano muscles in material tests.

Muscle material	Code	Test pressure (kPa)	Step response inertial mass (N)	Load cycle start tension (N)
60 μm LDPE	TP (Thin plastic)	30	9	10
125 μm LDPE	P (Plastic)	30	9	10
125 μm LDPE reinforced with 175 g m^{-2} polyester	PR (Plastic reinforced)	30	9	10
105 g m^{-2} polyester-silicone	TPC (Thin polyester composite)	200	40	40
175 g m^{-2} polyester-silicone	PC (Polyester composite)	200	40	40
175 g m^{-2} polyester-silicone (45-45 weave)	PCS (Polyester composite slanted weave)	200	15	40
25 g m^{-2} fiberglass-silicone	TFC (Thin fiberglass composite)	30	9	10
100 g m^{-2} fiberglass-silicone	FC (Fiberglass composite)	200	40	40

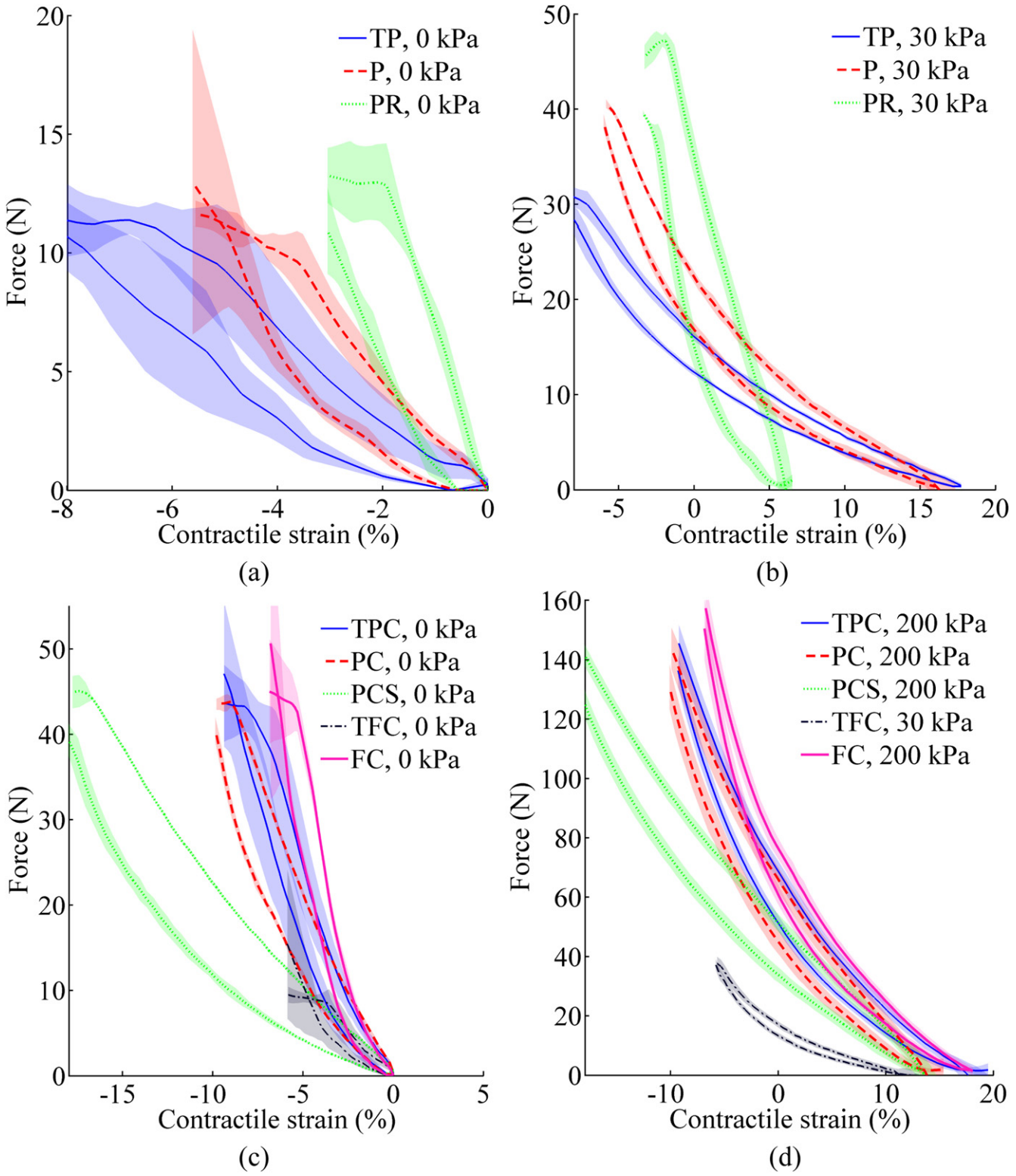

Figure 8. Load cycle curves of the plastic (a), (b) and textile-elastomer composite (c), (d) Peano muscles in unpressurized (a), (c) and pressurized (b), (d) states ($n = 6$). Refer to table 3 for the meaning of the material codes.

deformed significantly under these test conditions, reducing overall muscle stiffness. The higher test pressure meant that the blocking force of the 200 kPa muscles was higher, and correspondingly stretched the muscle mount tabs in a non-uniform manner. As shown in figure 10, the ends of the muscle's tubes were less loaded than its center, allowing them to contract more, and reducing the force transferred to the muscle load. A similar effect occurred with the plastic muscles at higher pressures due to stretching of their mount tab hole.

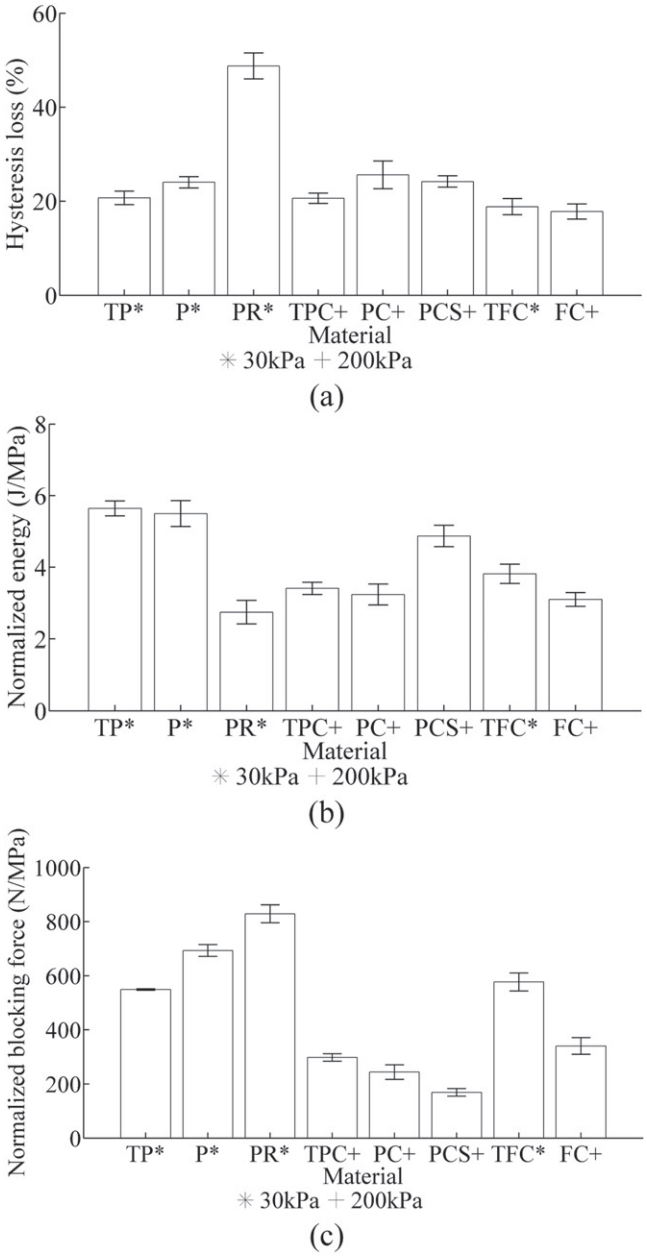

Figure 9. The effect of material on Peano muscle load cycle hysteresis (a), load cycle energy output (b), and blocking force (c) ($n = 6$). Refer to table 3 for the meaning of the material codes.

Figure 11(a) shows that the Peano muscles tested at 30 kPa inflated at speeds from fastest (0.03 m s^{-1}) to slowest (0.006 m s^{-1}) in the order of TP, P, TFC, and then PR. Muscles tested at 200 kPa tended to move faster overall with speeds starting at 0.027 m s^{-1} (PC) and followed by TPC, PCS, and FC (0.084 m s^{-1}). These trends are the result of the combined effect of flow restriction caused by channels, inertial mass size relative to actuation pressure, and free-strain. Out of the 30 kPa muscles, the more flexible plastic muscles had a higher speed because they not only had a greater free-strain, but also their channels inflated more easily, reducing flow restriction. The thin fiberglass muscle with its 3 mm high channels had no issues with channel flow

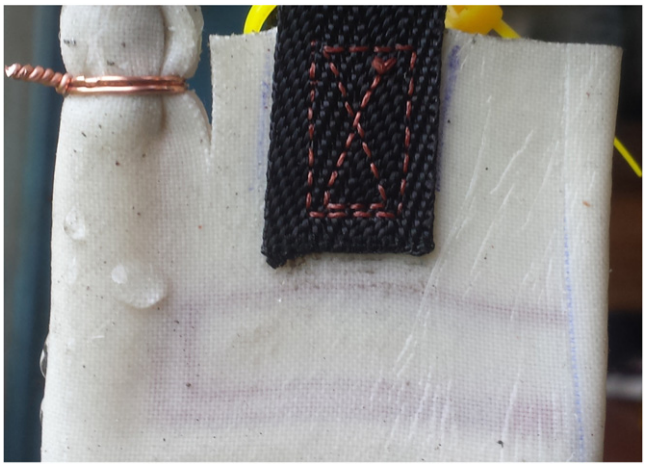

Figure 10. Nonuniform stretching of the coupling between the Peano muscle and its load.

restriction, but was less flexible than the P muscle, hence its slightly lower speed. The fiberglass (FC) muscle moved faster than the TPC and PC muscles as it produced the greatest blocking force to accelerate the 40 N load to a higher speed. The PCS muscle had the second highest speed despite its lower blocking force because it had a relatively lower inertial mass of 15 N. Overall, the 200 kPa muscles moved faster than the 30 kPa muscles because they had less flow restriction, a lower inertial mass to test pressure ratio, and higher free-strain at their test pressure.

Apart from the PCS muscle in figure 11(b) and the PCS and TFC muscles in figure 11(c), the normalized power and efficiency results follow the same trends as the muscle speeds. In figure 11(b), the muscle producing the highest power was FC with 19 W MPa^{-1}, and the least, PR with 2 W MPa^{-1}. The PCS muscle produces a similar amount of power to the PC muscle although it moves faster, as it has a lower inertial mass to perform work on. All the muscles in the 30 kPa tests have the same inertial mass and pressure, and consequently their efficiency trend reflects their blocking force and stroke capability, mirroring the trend of the speed and power results. Efficiency in these muscles ranges from 35% for the TP muscle to 8% for the muscle made from reinforced plastic. Peano muscles tested at 200 kPa span a similar range, with 32% for the FC muscle and 9% for the PCS and PC muscles. Again, within this subset of muscles, the trend is similar to that of power (and speed, apart from the PCS muscle with a lower inertial mass).

Experiments on the effect of using different materials in the Peano muscle have been very insightful to their future modeling, optimization, and application. They have emphasized the importance of tensile stiffness to blocking force, and bending stiffness (or some other proxy of material flexibility) to free-strain. They also show that both these stiffness components have losses that cause hysteresis. These losses are largely due to material viscoelasticity. Hence, results suggest a phenomenological model of the Peano muscle should be based on an ideal contractile unit in parallel with a viscoelastic element representing muscle tensile behavior, and in

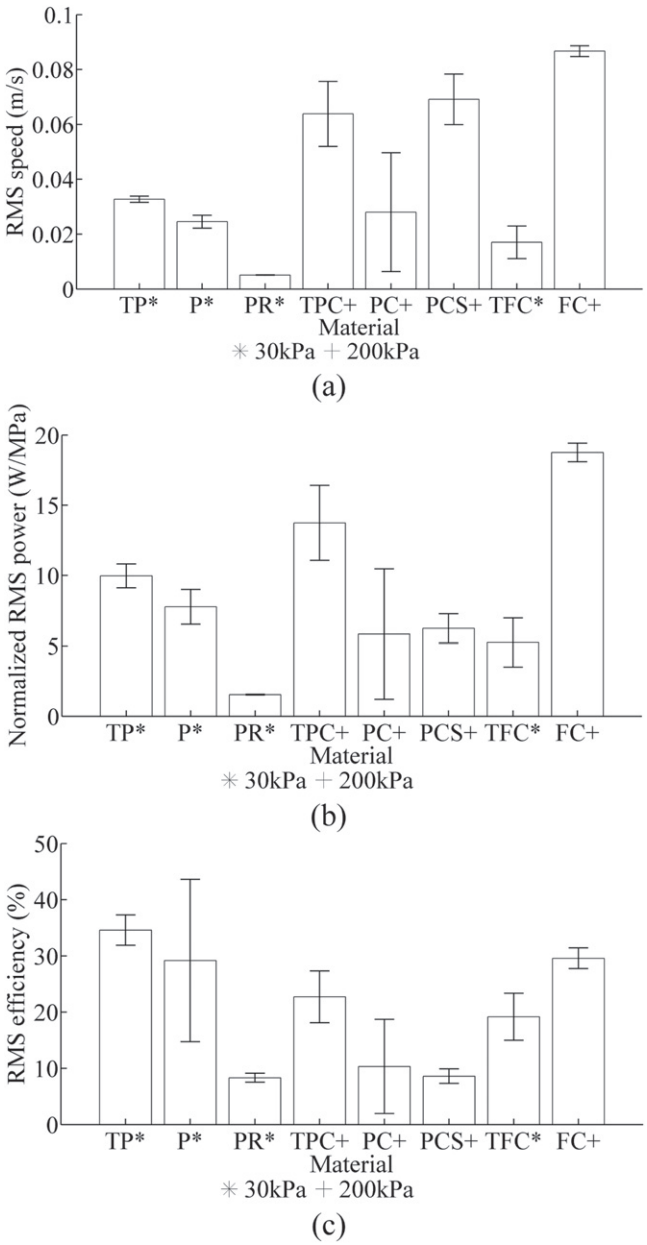

Figure 11. The effect of material on Peano muscle speed (a), power (b), and efficiency (c) ($n = 6$ except for efficiency where $4 \leqslant n \leqslant 6$). Refer to table 3 for the meaning of the material codes.

series with another representing the bending behavior of the muscle material. Due to the soft nature of the muscle a good starting point for the viscoelastic element are the Burgers and Zener models recommended by Case *et al* [25].

Friction is not an issue as it is in McKibben PAM as there is little relative movement between different materials in the Peano muscle. The load cycle experiments show that similar behavior is exhibited by stretchy and stiff polyester muscles and both could be modeled in the same way. The Peano muscle force can be maximized with the use of materials that are stiff in the length direction of the muscle. Its stroke and speed can be increased by using thin, highly flexible, and non-viscoelastic materials. Muscle power and efficiency can be optimized by using stiff, flexible materials with non-restrictive channels. Blocking force experiments and distortion of the muscle mount (figure 10) further demonstrate the importance of the coupling between the Peano muscle and its load. It must be stiff and distribute the load uniformly along the length of the muscle's tubes.

Experiments have shown that the SW Peano muscle, represented by the PCS muscle, is suitable for certain applications, such as gripping fragile objects and walking robots, where compliance (figures 8(c) and (d)) and energy storage (figure 9(b)) is desirable. In these cases, the SW Peano muscle can increase the compliance, energy storage, and range of motion of standard, relatively inextensible Peano muscles. We have shown how the material properties of Peano muscles affect their behavior and next we will discuss the implications of these observations on the capabilities and limitations of applying Peano muscles to actuation in soft or wearable robots.

5. Future applications

Although this study has not attempted to optimize the Peano muscle, it has provided enough insight on its behavior to compare its performance with other muscle-like actuators. Table 5 compares the static and dynamic characteristics of the 100 g m^{-2} fiberglass Peano muscle with PPAM [5], Festo PAM [5], nylon braid McKibben PAM [26–28], and mammalian skeletal muscle [28–31]. The muscles' actuation pressures and unstretched lengths (l_0) are given in the table column headings and energy, power, and maximum stress characteristics have been normalized by actuation pressure. All the characteristics are straightforward and have been taken directly from the above sources or calculated based on the data available. Entries marked as 'n/a' are not applicable to the given actuator, and those marked with a hyphen cannot be calculated from the available data. In stress and volume calculations, the maximum actuated area of the actuator and its unstretched length (inclusive of mounts) is used. Consistent with the results in this paper, the efficiency and average speed are specified for the muscle while is it delivering the listed average power figure. The (unoptimized and hydraulically actuated) fiberglass Peano muscle was chosen as the best overall performing muscle tested in this paper, biological muscle as the benchmark for soft and wearable actuation, and the other muscles are representative of high performing, pneumatically actuated, commercialized (McKibben PAM) and research prototype (McKibben PAM and PPAM) fluidic muscles.

5.1. Capabilities

The Peano muscle is efficient, responsive, and has an ideal physical form for actuating natural and artificial structures. Although its average power density and speed is down to one sixth of the nylon PAM, its power, speed, and efficiency are comparable to biological muscle, even at the relatively low 200 kPa pressures used in testing. The Peano muscle's speed and power can be further improved with higher pressure and

Table 5. Comparison of Peano muscle static and dynamic characteristics with PPAM, PAM, and biological muscle.

Property	FC Peano muscle @ 200 kPa ($l_0 = 0.06$)	PPAM @ 400 kPa ($l_0 = 0.04$)	Festo DMSP-10 @ 400 kPa ($l_0 = 0.04$)	Nylon PAM @ 500 kPa ($l_0 = 0.14$)	Biological muscle
Maximum stress (kPa)	550/MPa	1700/MPa	4100/MPa	1600/MPa	350
Free-strain (%)	18	38	13	25	40
Energy density (J kg^{-1})	51/MPa	182/MPa	36.5/MPa	67.5/MPa	83
Energy density (kJ m^{-3})	42.5/MPa	120/MPa	74/MPa	152/MPa	86
Load cycle hysteresis (%)	18	6	21	13	n/a
Threshold pressure (kPa)	<10	<10	100	100	n/a
Maximum thickness (m)	0.013	0.035	0.022	0.011	n/a
Average power density (W kg^{-1})	315/MPa	—	—	700/MPa	50
Average power density (kW m^{-3})	270/MPa	—	—	1580/MPa	52
Average speed (% s^{-1})	140	—	—	200	86
Dynamic efficiency (%)	32	—	—	<20	20–40

the use of air as the actuation fluid. However, air's compressibility reduces efficiency, as shown by the PAM's maximum dynamic efficiency being lower than the Peano muscle's. At slower actuation rates, the results of Meller *et al* [32] suggest that the quasistatic actuation of the hydraulically actuated Peano muscle could be in the range of 60%–80%. Meller *et al* [32] also found that PAM muscles with inextensible bladders, like the Peano muscle, have lower threshold pressures. Testing shows that similar to the PPAM, Peano muscles have a negligible threshold pressure, whereas typical PAMs have a threshold pressure of around 100 kPa.

Plainly, the most advantageous and unique characteristic of the Peano muscle is its ability to generate biologically significant power, force, and stroke in a thin and completely soft package. The Peano muscle, although unoptimized for minimum thickness, is thinner than the PPAM and Festo PAM, and only slightly thicker than the nylon PAM. However, unlike PAM, increasing its force only requires a wider, not a thicker, muscle. Thinner muscles can be made by reducing the muscle tube width (w_t), which will also increase the muscle's aspect ratio and hence stroke if the muscle material is flexible enough. The Peano muscle is made of discrete actuation chambers that increase its mechanical flexibility and versatility over a PPAM or PAM. Another feature that increases the versatility of the Peano muscle is the ability to configure it as a relatively inextensible or a stretchy actuator, depending on the alignment of its fibers. As a SW Peano muscle, such as the stretchy PCS muscle, it integrates the functionality of a nonlinear series elastic element into a fluidic muscle, even when it is hydraulically actuated.

These capabilities of the Peano muscle enable new possibilities for actuation. Its thin, soft, and high force generating form lend to the discreet and distributed actuation of existing structures, natural and artificial, fragile and tough. It can actuate load-bearing surfaces such as the human body, airframes, and vehicle and building surfaces. Potentially it is a step towards the 'active-anything' robotics paradigm that will intelligently automate the configuration and motion of everyday objects all around us. Compared to other fluidic muscles, the 2D form of the Peano muscle makes it easier to fabricate, handle, and apply to objects. While it does not possess extreme power, force, or precision capabilities, its combination of dynamic and static characteristics are well suited for working in and with the real world.

Apart from its form, independent pressurization of the discrete actuation chambers of the Peano muscle can be readily used to make variable recruitment and multi-degree-of-freedom actuators for superior force control, redundancy, and motion complexity [7, 33, 34]. Creating Peano muscles with multiple layers of muscle tubes enables them to bend. Lastly, the stretchable SW Peano muscle has integral and customizable passive elasticity. This muscle-like characteristic can be used for energy storage in dynamic applications such as an ankle orthosis, or compliance in grippers. It also enables a SW Peano muscle with its ends connected in a loop to be used as an adaptive coupling to soft bodies.

5.2. Limitations

Table 5 highlights that in comparison to biological muscle, PPAM, and PAM, the Peano muscle is limited by its lower maximum stress and free-strain, leading to a relatively low energy density. It also has a large hysteresis, and the experiments emphasized its poor robustness. Matching biological muscles' maximum stress would require a 640 kPa actuation pressure, and the Peano muscle produces 3–8 times less blocking force per unit pressure than either PPAMs or PAMs. A free-strain of 18% for the Peano muscle is less than half of the PPAM's 38% or biological muscles' 40%. It is also less than PAMs' free-strain of at least 25% (the Festo PAM only actuated to 13% as its stiff bladder requires 800 kPa to be contract by 25%). The experiments in this study and those of Niiyama *et al* [11] show that with the most flexible of materials the Peano muscle is unlikely to have a free-strain above 30% and is limited by its theoretical maximum free-strain of 36%. As with the PPAM, one of the aims of making the Peano muscle inextensible was to reduce its hysteresis compared to the PAM, making it easier to model and control. However, it had three times the 6% hysteresis of the PPAM and twice the hysteresis of the nylon PAM. The Festo PAM had a slightly higher hysteresis, again because it was operated at only half its maximum design pressure. Niiyama *et al*'s [9] Peano muscle had a lower hysteresis of 16%, but it was made out of more flexible plastic and operated at only 40 kPa.

In addition to these performance limitations, the Peano muscle prototypes lacked the robustness required of more demanding real world applications. We found that plastic Peano muscles are easy to fabricate, but readily puncture, stretch permanently, and burst at pressures of 100–200 kPa (125 μm LDPE muscles). This makes them good for exploring proof-of-concept designs and producing low cost, lightweight, and disposable actuators. Such an actuator could be useful in educational robotics [24], machines that handle food, or are involved in medical care. Reinforcing a plastic Peano muscle with a textile greatly increases its puncture resistance without significantly raising its cost, but in our prototype reduced its free-strain, increased its hysteresis, and had the extra risk of failure by delamination. Textile-elastomer composite muscles have the potential to be more robust, and we have successfully made leak-free composite Peano muscles that work at over 600 kPa. However, their construction needs improvement as they tend to develop pinhole leaks around the stitching and this leads to delamination of the outer textile wrap. Also, fiberglass is not a suitable textile because it is too brittle and breaks where it is flexed along stitching seams. It was only used in this study as it was a readily available example of a very stiff textile.

This study did not aim to optimize the Peano muscle and there are a few options for improving its static characteristics. Stiffer and stronger textiles based on fibers such as Zylon, Kevlar, or Dyneema will increase the maximum stress of composite Peano muscles and enable them to operate at higher pressures. Mori *et al* [23] have shown that by using the stiff poly(p-phenylene-2,6-benzobisoxazole)) (PBO) fibers of Zylon with hydraulic actuation can produce very high forces

at pressures of 4 MPa. Essential to realizing these stresses is a stiff, flexible mount that uniformly loads the whole length of the Peano muscle tubes. Such a mount will also allow Peano muscles to transfer more motion to their load. Increasing free-strain closer to the theoretical limit needs thin, flexible muscle materials. Another way to get more motion out of the Peano muscle is to use it with a strain amplifying lever mechanism. Alternatively, continuous long-stroke motion can be obtained by independently actuating muscle tubes pressed against a stiff, flexible film in a peristaltic sequence. A similar concept has been applied to multiple PAMs in a tube [35]. The wave motion in the Peano muscle tubes will move the film relative to the muscle in a direction and speed dependent on the tube pressurization sequence. However, these latter approaches compromise the simplicity and monolithic nature of the Peano muscle. Therefore, while we acknowledge that the Peano muscle's physics may prevent it from generating the motion required in some applications, its inherently limited stroke is an advantage for moderate stroke applications that need a low force at their end of travel for safety reasons. Examples include robotic prosthetics, orthotics, search and rescue robots, and produce harvesting and handling equipment.

Hysteresis of Peano muscles can be improved with a stiff, uniform coupling between the muscle and its load. Additionally, flexible non-viscoelastic materials and stiff, non-rearranging textiles will reduce hysteresis. If a Peano muscle can be made with the flexibility of the textile-plastic membrane of PPAMs, both its hysteresis and robustness could be potentially improved. The reason that composite Peano muscles were prone to leaking is their use of stitching to hold layers of textile together. We recommend that the robustness of these muscles be improved by eliminating stitching. Two solutions are either to make the muscle tubes from woven textile tubes cut to length, or to weave ribbons of textile along the length of the muscle, above and below alternate muscle tubes. Both techniques will ensure the textile is loaded in tension along its whole length without the out-of-plane stress concentrations introduced by stitches. Finally, the muscles rigid fittings should be replaced with flexible reinforced hosing to minimize the stress concentrations that occur between the fittings and soft muscle.

6. Conclusions

The soft, thin form of the Peano muscle is ideal for responsive and discreet actuation of soft and rigid bodies. It is however, limited by its free-strain, which is typically between 15% and 30%. We have found that actuated Peano muscles are ideally made of stiff, flexible, and non-viscoelastic materials. Critical to their performance is a stiff coupling to their load across the length of the muscle tube. Sarosi's force model is most suitable for modeling the pressurized behavior of the Peano with an RMSE of 10.2 N. The dynamic model of Sarosi *et al* tends to overestimate oscillation frequency and damping and with an RMSE of 2.6% strain is only recommended as a first approximation of muscle behavior. As a potential improvement, we suggest the Peano muscle be modeled by a parallel ideal contractile unit and viscoelastic element, both in series with another viscoelastic element.

The next step in this work is to optimize the Peano muscle for application to a wearable robot such as a soft wrist orthosis. This will require a more advanced dynamic phenomenological model to be developed, further tests on stiff flexible materials, and evaluation of scalable fabrication techniques that maximize muscle robustness.

Acknowledgments

A J Veale appreciatively recognizes the support of The University of Auckland Doctoral Scholarship and thanks Dean Veale for his assistance with carrying out experiments on the Peano muscles.

References

[1] Klamroth-Marganska V *et al* 2014 Three-dimensional, task-specific robot therapy of the arm after stroke: a multicentre, parallel-group randomised trial *Lancet Neurol.* **13** 159–66
[2] Pohl M, Warner C, Holzgraefe M, Kroczek G, Mehrholz J, Wingerdorf I, Hölig G, Koch R and Hesse S 2007 Repetitive locomotor training and physiotherapy improve walking and basic activities of daily living after stroke: a single-blind, randomised multicentre trial (DEutsche GAngtrainerStudie, DEGAS) *Clin. Rehabil.* **21** 17–27
[3] Veale A J and Xie S Q 2016 Towards compliant and wearable robotic orthoses: a review of current and emerging actuator technologies *Med. Eng. Phys.* **38** 317–25
[4] Daerden F 1999 Conception and realization of pleated pneumatic artificial muscles and their use as compliant actuation elements *PhD Dissertation* Vrije Universiteit Brussel
[5] Villegas D, Van Damme M, Vanderborght B, Beyl P and Lefeber D 2012 Third-generation pleated pneumatic artificial muscles for robotic applications: development and comparison with mckibben muscle *Adv. Rob.* **26** 1205–27
[6] Davis S, Canderle J, Artrit P, Tsagarakis N and Caldwell D G 2002 Enhanced dynamic performance in pneumatic muscle actuators *IEEE Int. Conf. on Robotics Automation (Washington, DC)* pp 2836–41
[7] Bryant M, Meller M A and Garcia E 2014 Variable recruitment fluidic artificial muscles: modeling and experiments *Smart Mater. Struct.* **23** 1–12
[8] Sanan S, Lynn P S and Griffith S T 2014 Pneumatic torsional actuators for inflatable robots *J. Mech. Robot.* **6** 1–7
[9] Niiyama R, Sun X, Sung C, An B, Rus D and Kim S 2015 Pouch motors: printable soft actuators integrated with computational design *Soft Robot.* **2** 59–70
[10] Veale A J, Anderson I A and Xie S Q 2015 The smart peano fluidic muscle: a low profile flexible orthosis actuator that feels pain *SPIE Smart Structures and Materials NDE (San Diego, CA)* pp 94351V-1-11
[11] Niiyama R, Rus D and Kim S 2014 Pouch motors: printable/inflatable soft actuators for robotics *IEEE Int. Conf. on Robotics Automation (Hong Kong)* pp 6332–7
[12] Park Y, Santos J, Galloway K G, Goldfield E C and Wood R J 2014 A soft wearable robotic device for active knee motions using flat pneumatic artificial muscles *IEEE Int. Conf. on Robotics Automation (Hong Kong)* pp 4805–10
[13] Sárosi J 2012 New approximation algorithm for the force of fluidic muscles *7th IEEE Int. Symp. on Applied Computational Intelligence and Informatics (Timisoara, Romania)* pp 229–33

[14] Sárosi J, Biro I, Nemeth J and Cveticanin L 2015 Dynamic modeling of a pneumatic muscle actuator with two-direction motion *Mech. Mach. Theory* **85** 25–34
[15] Sangian D, Naficy S, Spinks G M and Tondu B 2015 The effect of geometry and material properties on the performance of a small hydraulic McKibben muscle system *Sensors Actuators* A **234** 150–7
[16] Pillsbury T E, Kothera C S and Wereley N M 2015 Effect of bladder wall thickness on miniature pneumatic artificial muscle performance *Bioinspir. Biomimetics* **10** 1–15
[17] Niiyama R, Rognon C and Kuniyoshi Y 2015 Printable pneumatic artificial muscles for anatomy-based humanoid robots *IEEE-RAS 15th Int. Conf. Humanoid Robots (Seoul, Korea)* pp 401–6
[18] Chang S Y, Takashima K, Nishikawa S, Niiyama R, Someya T, Onodera H and Kuniyoshi Y 2015 Design of small-size pouch motors for rat gait rehabilitation device *Proc. Annu. Int. Conf. IEEE Engineering in Medicine and Biology Society EMBS (Milan, Italy)* pp 4578–81
[19] Reynolds D B, Repperger D W, Phillips C A and Bandry G 2003 Modeling the dynamic characteristics of pneumatic muscle *Ann. Biomed. Eng.* **31** 310–7
[20] Cao J, Xie S Q, Zhang M and Das R 2014 A new dynamic modelling algorithm for pneumatic muscle actuators *Lect. Notes Comput. Sci.* **8918** 432–40
[21] Tondu B 2013 Use of textile friction to mimic hill's model in dynamic contraction of braided artificial muscles *Adv. Sci. Technol.* **84** 39–44
[22] Klute G K and Hannaford B 1998 Fatigue characteristics of McKibben artificial muscle actuators *IEEE Int. Conf. Intell. Robots Syst. (Victoria, BC)* pp 1776–81
[23] Mori M, Suzumori K, Takahashi M and Hosoya T 2010 Very high force hydraulic McKibben artificial muscle with a p-phenylene-2,6-benzobisoxazole cord sleeve *Adv. Rob.* **24** 233–54
[24] Niiyama R, Sun X, Yao L, Ishii H, Rus D and Kim S 2015 Sticky actuator: free-form planar actuators for animated objects *9th Int. Conf. Tangible, Embedded, and Embodied Interaction (Stanford, CA)* pp 77–84
[25] Case J C, White E L and Kramer R K 2015 Soft material characterization for robotic applications *Soft Robot.* **2** 80–7
[26] Woods B K S, Gentry M F, Kothera C S and Wereley N M 2012 Fatigue life testing of swaged pneumatic artificial muscles as actuators for aerospace applications *J. Intell. Mater. Syst. Struct.* **23** 327–43
[27] Robinson R M, Kothera C S, Woods B K S, Vocke R D and Wereley N M 2011 High specific power actuators for robotic manipulators *J. Intell. Mater. Syst. Struct.* **22** 1501–11
[28] Chou C and Hannaford B 1996 Measurement and modeling of McKibben pneumatic artificial muscles *IEEE Trans. Robot. Autom.* **12** 90–102
[29] Hunter I W and Lafontaine S 1992 A comparison of muscle with artificial actuators *IEEE 5th Solid-State Sensor and Actuator Workshop Tech. Dig. (Hilton Head Island, SC)* pp 178–85
[30] Madden J D W, Vandesteeg N A, Anquetil P A, Madden P G A, Takshi A, Pytel R Z, Lafontaine S R, Wieringa P A and Hunter I W 2004 Artificial muscle technology: physical principles and naval prospects *IEEE J. Ocean. Eng.* **29** 706–28
[31] Hannaford B and Winters J M 1990 Actuator properties and movement control: biological and technological models *Multiple Muscle Systems: Biomechanics and Movement Organization* ed J M Winters and S L Soo (New York: Springer) pp 101–20
[32] Meller M A, Bryant M and Garcia E 2014 Reconsidering the McKibben muscle: energetics, operating fluid, and bladder material *J. Intell. Mater. Syst. Struct.* **25** 2276–93
[33] Robinson R M, Kothera C S and Wereley N M 2014 Variable recruitment testing of pneumatic artificial muscles for robotic manipulators *IEEE Trans. Mechatron.* **20** 1642–52
[34] Mathijssen G, Schultz J, Vanderborght B and Bicchi A 2015 A muscle-like recruitment actuator with modular redundant actuation units for soft robotics *Robot. Auton. Syst.* **74** 40–50
[35] Saga N, Nakamura T and Ueda S 2003 Study on peristaltic crawling robot using artificial muscle actuator *IEEE Int. Conf. Advanced Intelligent Mechatronics (Kobe, Japan)* pp 679–84